J Therm Anal Calorim (2012) 107:527–533
DOI 10.1007/s10973-011-1607-5

The effect of water molecule on the thermal stability of lanthanide compounds with 1,3-benzeneditetrazol-5-yl

Cheng-Fang Qiao · Qing Wei · Zheng-Qiang Xia · Chun-Sheng Zhou · San-Ping Chen

Received: 29 January 2011 / Accepted: 19 April 2011 / Published online: 5 May 2011

Abstract Six lanthanide compounds $[Ln(H_2O)_9](m\text{-}BDTH)_3{\cdot}9(H_2O)$ where Ln = La (**1**), and $[Ln(H_2O)_8](m\text{-}BDTH)_3{\cdot}9(H_2O)$ (*m*-$BDTH_2$ = 1,3-benzeneditetrazol-5-yl) where Ln = Lu (**2**), Yb (**3**), Er (**4**), Ho (**5**) and Y (**6**) were hydrothermally synthesized and characterized by elemental analyses, infrared spectra, powder X-ray diffraction (PXRD) and X-ray single crystal diffraction. PXRD indicates that **2**–**6** are isomorphous. Structural analyses reveal that **1** is coordinated by nine water molecules forming a capped-square antiprism, while **2**–**6** are coordinated by eight water molecules forming a simple square antiprismatic geometry. Effects of water molecules on thermal stability were also discussed by thermogravimetric (TG), DSC, and PXRD under different temperatures. TG analyses suggest that **1** loses lattice and coordinated water molecules with no diacritical boundary, and **6** removes lattice water molecules first and then coordinated water molecules. DSC and PXRD further confirm the consequence.

Keywords Intermolecular interaction · Lanthanide compound · 1,3-Benzeneditetrazol-5-yl · Thermal stability

C.-F. Qiao · Q. Wei (✉) · Z.-Q. Xia · S.-P. Chen (✉)
Key Laboratory of Synthetic and Natural Functional Molecule Chemistry of Ministry of Education, College of Chemistry and Materials Science, Northwest University, Xi'an 710069, China
e-mail: sanpingchen@126.com

C.-F. Qiao · C.-S. Zhou
Department of Chemistry, Shangluo University, Shangluo 726000, China

Introduction

The intermolecular interactions including hydrogen-bonds, halogen–halogen interactions, π–π contacts, van der Waals forces, are key in the crystal engineering of organic solids [1, 2] as well inorganic and organic moieties [3–6]. Particularly, the hydrogen-bonding interaction has emerged to be a powerful tool for the molecular assembly due to its suitable strength and directionality [7], and the design of supramolecular systems based on noncovalent synthesis [8–10]. Furthermore, many theoretical and experimental studies [11, 12] provide novel structural aspects of water and new insights into the behavior of water with implications in biology and environment.

Tetrazoles are heterocyclic compounds that exhibit properties of both acids and bases [13] and have comparable p*K*a values to the corresponding carboxylic acids (RCO_2H) [14]. They can act as ligands in metal complexes, form salts, and can be both acceptors and donors for hydrogen-bonding. Thus, the 1,3-benzeneditetrazol-5-yl (*m*-$BDTH_2$) serves as either multidentate or bridge building block in supramolecular assembly exhibiting both great structural diversities as well as catalysis, gas absorption, non-linear optics, ion-exchange, luminescence, and magnetism [15–18].

Due to the effect of lanthanide contraction, the chemical property of yttride is very similar to lanthanide. Herein, a series of compounds based on *m*-$BDTH_2$ with 2-D hydrophobic [19] organic layers of π-stacked and hydrogen-bonded $(m\text{-}BDTH)^-$ and hydrophilic $[Ln(H_2O)_n]^{3+}$ cationic pillars depending on rare earth metal cation, had been prepared by the solvothermal route. We report the structural characterization, and comparison of six Ln^{3+} compounds: $[Ln(H_2O)_9](m\text{-}BDTH)_3{\cdot}9(H_2O)$ where Ln = La (**1**), and $[Ln(H_2O)_8](m\text{-}BDTH)_3{\cdot}9(H_2O)$ where Ln = Lu (**2**), Yb (**3**),

Er (**4**), Ho (**5**), and Y (**6**). The compounds **1**–**6** exhibit hydrophilic cationic coordination frameworks $[Ln(H_2O)_n]^{3+}$ that encapsulate uncoordinated (*m*-BDTH)$^-$ anions and water molecules. Furthermore, we discuss the effects of water molecules on thermal stability of **1**–**6** by TG, DSC, and PXRD analyses under different temperatures.

Experimental

Materials and measurements

All reagents were purchased commercially and used without further purification.

Elemental analyses were carried out with an Elementar Vario EL III analyzer. IR spectra were recorded with a Tensor 27 spectrometer (Bruker Optics, Ettlingen, Germany). Thermogravimetric measurements were performed with a Netzsch STA449C apparatus under a nitrogen atmosphere with a heating rate of 10 °C min^{-1} from 30 to 800 °C. DSC experiments were performed using a CDR-4P thermal analyzer of Shanghai Balance Instrument factory under a flow of 100 mL min^{-1} nitrogen from 30 to 500 °C. The powder X-ray diffraction (PXRD) patterns were measured on a Bruker D8 Advance diffractometer.

All single crystal X-ray experiments were performed on a Bruker Smart Apex CCD diffractometer equipped with graphite monochromatized Mo *Kα* radiation (λ = 0.71073 Å) using ω and φ scan mode. The single-crystal structures of complexes were both solved by direct methods and refined with full-matrix least squares refinements based on F^2 using SHELXS-97 and SHELXL-97 [20, 21]. All non-hydrogen atoms were refined anisotropically. Crystallographic data are summarized in Table 1, selected bond lengths are shown in Table 2, and selected hydrogen bonding interactions are shown in Table 3 for **1** and **6**.

Syntheses

*Synthesis of $[La(H_2O)_9](m\text{-}BDTH)_3{\cdot}9(H_2O)$ (**1**)*

m-$BDTH_2$ was synthesized according to the literature [22]. A mixture of $LaCl_3$ (0.1470 g, 0.5 mmol), *m*-$BDTH_2$ (0.1071 g, 0.5 mmol), were suspended in the solution of H_2O (5 mL), and heated in a 10 mL Teflon-lined steel bomb at 160 °C for 3 days. After the sample was cooled to room temperature at a rate of 10 °C h^{-1}, the colorless prismy crystals formed were collected, washed with water, and dried in air. Yield: 64%. IR (KBr, cm^{-1}): 3371(br, s), 2417(m), 1662(s), 1651(m), 1599(m), 1451(m), 1419(m), 1381(w), 1334(w), 1253(w), 1220(w), 1176(m), 1041(m), 1040(m), 989(m), 907(w), 763(m), 736(m), 692(w). Anal. Calcd. $C_{24}H_{49}N_{24}O_{17}La$ weight (%): C, 25.72; N, 29.99; H, 4.41. Found: C, 25.81; N, 30.12; H, 4.53.

Table 1 Crystal data and structure refinement summary for **1** and **6**

Empirical formula	$C_{24}H_{51}N_{24}O_{18}La$	$C_{24}H_{49}N_{24}O_{17}Y$
Formula weight	1102.80	1034.78
Crystal system	Triclinic	Triclinic
Space group	*P*-1	*P*-1
a/Å	9.863 (3)	9.873 (5)
b/Å	13.273 (4)	13.892 (7)
c/Å	17.248 (5)	16.716 (8)
α/°	80.632 (4)	79.873 (8)
β/°	80.102 (4)	76.814 (7)
γ/°	88.661 (4)	78.316 (7)
V/Å^3	2.1947 (11)	2.1656 (19)
Z	2	2
ρ_{calc}/g cm^{-3}	1.669	1.587
μ/mm^{-1}	1.072	1.443
F(000)	1128	1072
θ/°	2.10–25.00	1.83–25.10
$R_{(int)}$	0.0442	0.0717
Goodness-of-fit on F^2	1.012	1.111
Final *R* indices [$I > 2\sigma(I)$]	$R_1 = 0.0731$, $wR_2 = 0.2005$	$R_1 = 0.0991$, $wR_2 = 0.2408$
R indices (all data)	$R_1 = 0.1035$, $wR_2 = 0.2446$	$R_1 = 0.1648$, $wR_2 = 0.2811$
Largest diff. peak and hole (e Å^{-3})	1.242 and −1.373	1.173 and −1.279

Table 2 Selected bond lengths (Å) for **1** and **6**

Compound 1					
La(1)–O(1)	2.562 (8)	La(1)–O(2)	2.573 (8)	La(1)–O(3)	2.507 (6)
La(1)–O(4)	2.591 (6)	La(1)–O(5)	2.554 (6)	La(1)–O(6)	2.569 (7)
La(1)–O(7)	2.590 (8)	La(1)–O(8)	2.580 (8)	La(1)–O(9)	2.533 (6)
Compound 6					
Y(1)–O(2)	2.335 (6)	Y(1)–O(8)	2.340 (7)	Y(1)–O(7)	2.348 (6)
Y(1)–O(4)	2.362 (6)	Y(1)–O(3)	2.374 (6)	Y(1)–O(6)	2.374 (6)
Y(1)–O(1)	2.381 (6)	Y(1)–O(5)	2.397 (6)		

Table 3 Hydrogen bonding interactions in **1** and **6**

D–H···A	D–H/Å	H···A /Å	D···A/Å	∠DHA/°
Compound 1[a]				
N(8)–H(8)···O(2)#1	0.86	2.11	2.872 (11)	147.3
N(16)–H(16)···O(10)#2	0.86	2.04	2.803 (15)	147.4
N(21)–H(21A)···O(5)	0.86	2.05	2.832 (10)	151.1
O(1)–H(1A)···O(15)	0.85	2.53	3.33 (3)	157.8
O(7)–H(7N)···N(1)#3	0.85	2.23	3.014 (12)	153.8
O(7)–H(7B)···N(10)#3	0.85	2.29	3.049 (12)	149.3
O(8)–H(8A)···N(9)#3	0.85	2.03	2.745 (11)	141.7
O(9)–H(9A)···N(5)#3	0.85	2.11	2.935 (9)	163.8
O(9)–H(9B)···N(3)#4	0.85	2.01	2.826 (9)	161.0
Compound 6[b]				
O(6)–H(6A)···O(15)#1	0.85	1.97	2.802 (13)	166.3
O(4)–H(4B)···O(2)	0.85	2.23	3.026 (9)	155.5
O(4)–H(4A)···O(16)	0.85	2.14	2.947 (17)	158.8
O(2)–H(2A)···N(21)	0.85	2.03	2.748 (8)	141.1
O(1)–H(1B)···N(21)	0.85	2.55	3.321 (9)	152.1
N(18)–H(18)···N(23)#2	0.86	1.94	2.766 (9)	161.4
N(15)–H(15N)···O(14)	0.86	2.04	2.876 (12)	162.7
N(4)–H(4N)···N(8)#2	0.86	1.92	2.754 (9)	163.2

[a] Symmetry operations: #1 $x, y, z-1$; #2 x, $y-1, z$; #3 $-x+1, -y+1, -z+1$; #4 $-x, -y+1, -z+1$

[b] Symmetry operations: #1 $x, y-1, z$; #2 $x+1, y, z$

Synthesis of [Lu(H₂O)₈](m-BDTH)₃·9(H₂O) (2)

2 was prepared by the procedure similar to that of **1** except that $LaCl_3$ was replaced by $LuCl_3$. Yield: 65%. IR (KBr, cm^{-1}): 3356(br, s), 2417(m), 1660(s), 1650(m), 1576(m), 1451(m), 1411(w), 1385(w), 1335(w), 1255(w), 1216(w), 1161(m), 1087(m), 1041(m), 994(m), 903.7(w), 767(m), 736(m), 683(w). Anal. Calcd. $C_{24}H_{49}N_{24}O_{17}Lu$ weight (%): C, 25.72; N, 29.99; H, 4.41. Found: C, 25.81; N, 30.12; H, 4.53.

Synthesis of [Yb(H₂O)₈](m-BDTH)₃·9(H₂O) (3)

3 was prepared by the procedure similar to that of **1** except that $LaCl_3$ was replaced by $YbCl_3$. Yield: 74%. IR (KBr, cm^{-1}): 3352(br, s), 2420(m), 1662(s), 1653(m), 1579(m), 1456(m), 1411(w), 1385(w), 1337(w), 1255(w), 1218(w), 1161(m), 1088(m), 1041(m), 994(m), 904(w), 767(m), 739(m), 683(w). Anal. Calcd. $C_{24}H_{49}N_{24}O_{17}Yb$ weight (%): C, 25.76; N, 30.05; H, 4.41. Found: C, 25.89; N, 30.12; H, 4.52.

Synthesis of [Er(H₂O)₈](m-BDTH)₃·9(H₂O) (4)

4 was prepared by the procedure similar to that of **1** except that $LaCl_3$ was replaced by $Er(NO_3)_3$. Yield: 68%. IR (KBr, cm^{-1}): 3370(br, s), 2417(m), 1662(m), 1608(m), 1455(m), 1422(m), 1384(m), 1328(w), 1254(w), 1219(w),1179(m), 1086(m), 1041(m), 979(m), 905(m), 763(s), 732(m), 681(w). Anal. Calcd. $C_{24}H_{49}N_{24}O_{17}Er$ weight (%): C, 25.90; N, 30.20; H, 4.44. Found: C, 26.05; N, 30.32; H, 4.61.

Synthesis of [Ho(H₂O)₈](m-BDTH)₃·9(H₂O) (5)

5 was prepared by the procedure similar to that of **1** except that $LaCl_3$ was replaced by $Ho(NO_3)_3$. Yield: 62%. IR (KBr, cm^{-1}): 3300(br, s), 2426(m), 1662(s), 1651(m), 1577(m), 1428(m), 1384(w), 1334(w), 1253(w), 1219(w), 1176(m), 1078(m), 1049(m), 989(m), 905(m), 771(m), 736(m), 681(w). Anal. Calcd. $C_{24}H_{49}N_{24}O_{17}Ho$ weight (%): C, 25.95; N, 30.26; H, 4.45. Found: C, 26.02; N, 30.30; H, 4.60.

Synthesis of [Y(H₂O)₈](m-BDTH)₃·9(H₂O) (6)

6 was prepared by the procedure similar to that of **1** except that $LaCl_3$ was replaced by $Y(NO_3)_3$. Yield: 61%. IR (KBr, cm^{-1}): 3299(br, s), 2462(m), 1662(w), 1599(m), 1572(m), 1455(m), 1428(m), 1384(w), 1329(w), 1253(w), 1221(w), 1167(m), 1086(m), 1041(m), 997(m), 907(w), 763(m),

736(m), 689(w). Anal. Calcd. $C_{24}H_{49}N_{24}O_{17}Y$ weight (%): C, 27.86; N, 32.49; H, 4.77. Found: C, 27.91; N, 32.61; H, 4.90.

Results and discussion

Syntheses and PXRD

Metal-tetrazole-based materials have received considerable attention in the past decades, however, the polymeric phases generally occur as insoluble polycrystalline powders. Undoubtedly, the hydrothermal synthesis affords a convenient method for preparation of such composite materials, allowing more routine structural characterization by single crystal X-ray diffraction [23, 24].

Similar to the previously described compounds [19], for **1–6** the tetrazole-based ligands are present in singly deprotonated $(m\text{-BDTH})^-$ organic monoanion form. Compared with those in the literatures, we provided a more convenient and mild condition for syntheses of **1–6**. PXRD indicates that **2–6** are isomorphous (Fig. 1).

Crystal structures of **1** and **6**

The structures of **1** and **6** were determined using single-crystal X-ray diffraction. Both **1** and **6** crystallize in space groups *P*-1. The asymmetric units each contain one lan-

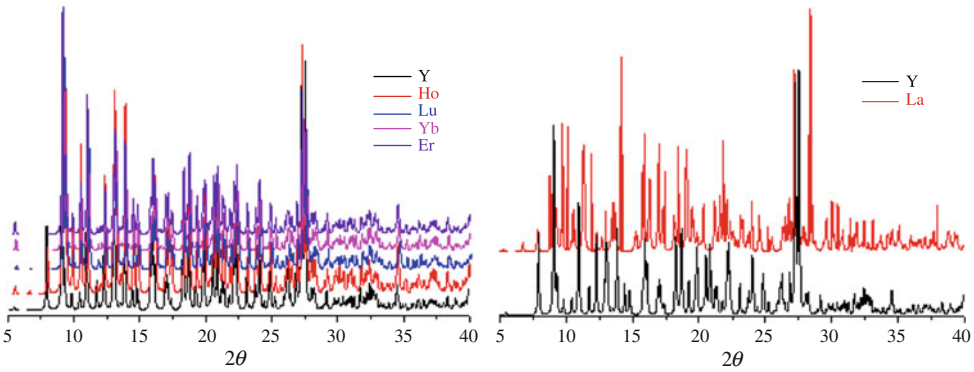

Fig. 1 (*left*) X-ray powder patterns calculated for **6** and measured for compounds **2–5**; (*right*) X-ray powder patterns calculated for **1** and **6**

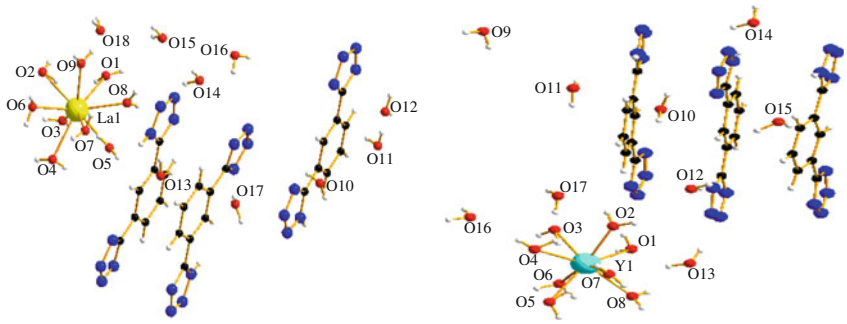

Fig. 2 Views of the asymmetric units **1** (*left*) and **6** (*right*)

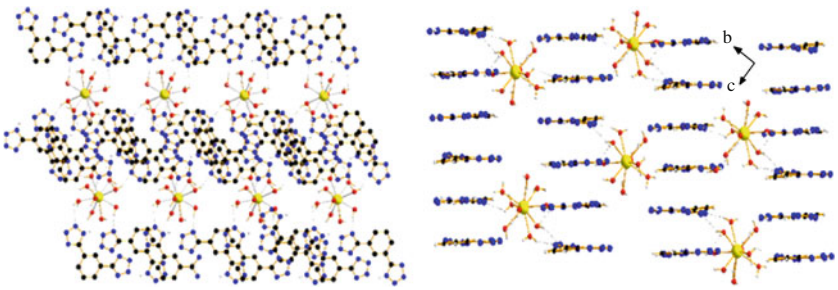

Fig. 3 The three-dimensional framework of **1**, viewed down the *a* axis (*left*) and projected onto the $(0\bar{1}1)$ plane (*right*), showing the H-bonding between the coordinated waters and the organic anions. La *yellow*, O *red*, N *blue*, C *black*. The lattice water molecules are omitted for clarity

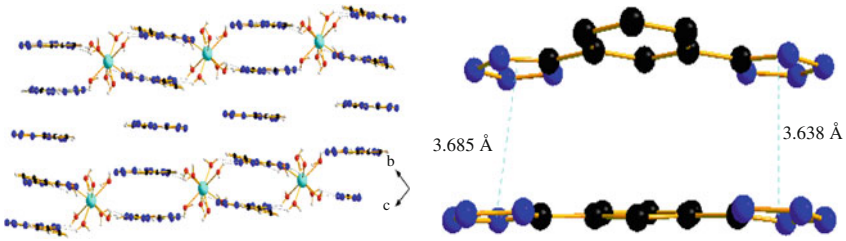

Fig. 4 The three-dimensional framework of **6**, viewed down the *a* axis (*left*) and π–π stacking interactions of the tetrazole rings in **6** (*right*). Y *turquiose*, O *red*, N *blue*, C *black*

thanide aqua complex trication, three singly deprotonated (*m*-BDTH)$^-$ organic monoanions, and nine lattice water molecules so that both compounds are hydrated salts. In **1**, La(1) is coordinated by nine water molecules forming a capped-square antiprism, with the eight La–O distances within the antiprism in the range 2.533(6)–2.591(6) Å and the distance to the capping oxygen 2.507(6) Å. In **6**, Y(1) is coordinated by eight water molecules forming a simple square antiprismatic geometry, with the Y–O bond lengths in the range 2.335(6)–2.397(6) Å (see Fig. 2 and Table 2).

The structures of **1** and **6** are each constructed from 2D layers of organic anions separated by mononuclear lanthanide complex pillars resulting in a three-dimensional framework. The structure of **1** is shown in Fig. 3, while that of **6** is shown in Fig. 4.

The single deprotonated aromatic rings lead to the expected hydrogen-bonding and π–π stacking interactions. The planes of the *m*-BDTH$^-$ ligands are parallel with each other, and are stacked such that the distances between planes are close. Set **6** for an example, the C13–N13–N14–N15 and C6–N1–N2–N3 tetrazole rings are involved in offset face-to-face π–π interactions with centroid–centroid separation 3.685 Å, while the C9–N9–N12–N11 and C1–N5–N8–N6 tetrazole rings have centroid–centroid separation 3.638 Å (Fig. 4), they both exhibit strong π–π stacking interactions. In this way, hydrophobic organic layers are formed, parallel to the (001) and (011) planes for **1** and **6**, respectively. The water ligands on the lanthanide cations form a total of eight hydrogen bonds between adjacent hydrophobic layers [19], thereby constituting the hydrophilic pillars.

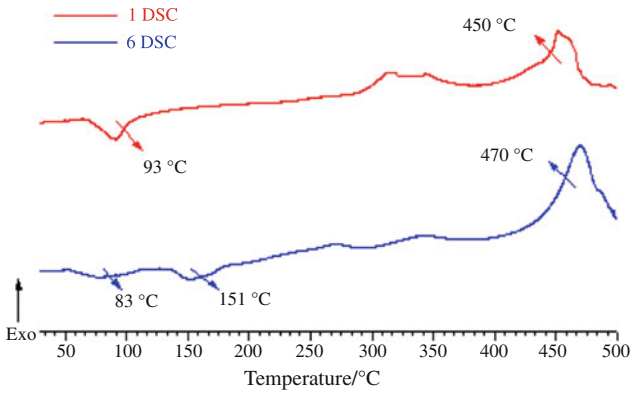

Fig. 6 DSC curves of **1** and **6** with the heating rate 10 °C min^{-1}

Thermal stability analyses

TG analyses were performed between 30 and 800 °C at a heating rate of 10 °C min^{-1}, in nitrogen atmosphere. As shown in Fig. 5, TG curves of **2**–**6** are very similar with the explanation that they are isomorphous. Consequently, we only describe thoroughly thermogravimetric performances of two representative samples (**1** and **6**) (see Fig. 6). The two compounds reveal slightly different thermal behavior.

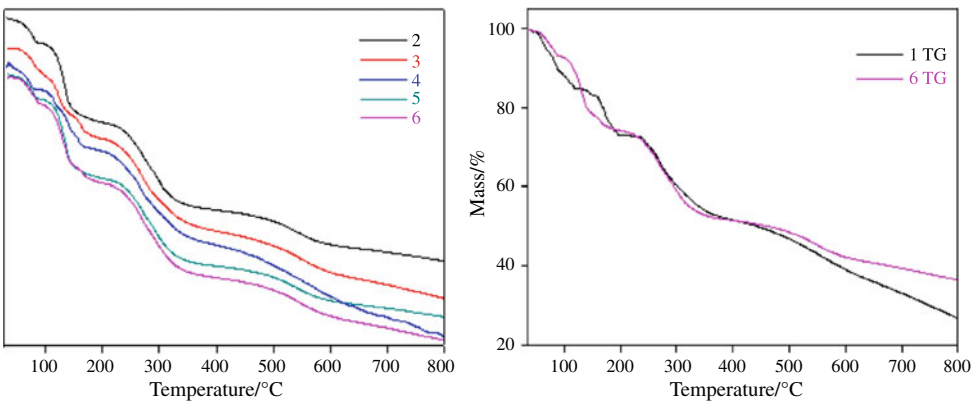

Fig. 5 TG curves of **2**–**6** (*left*) (the vertical coordinate is omitted and TG curves of **2**–**6** are separated for clarity) and **1** and **6** (*right*) with the heating rate 10 °C min^{-1}

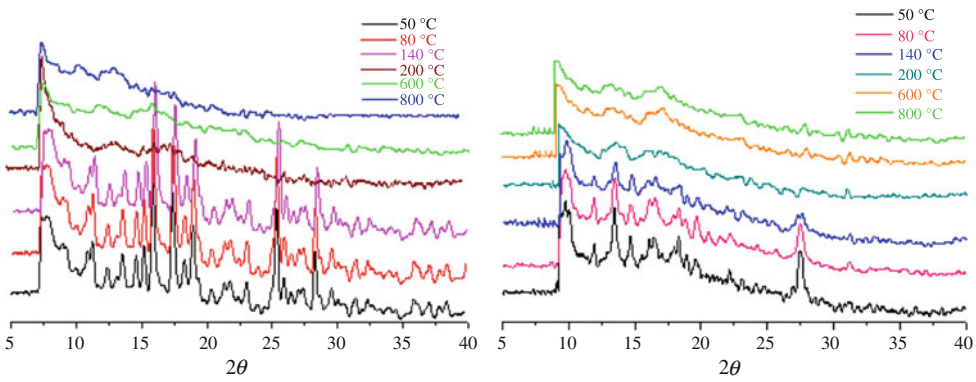

Fig. 7 PXRD patterns of **1** (La) (*left*) and **6** (Y) (*right*) calcined at different temperatures

For **1**, there is no diacritical boundary for loss of lattice and coordinated water molecules, which are all lost below 200 °C. The removal of water molecules takes place in one endothermic process in which the calculated value for 18 water molecules (28.91%) differs with the experimental value (26.07%), indicating that two water molecules attaches to the La^{3+} center still remain in the partially dehydrated compound. TGA reveals that the residue is not a stable substance, in addition, flat curve of PXRD at 800 °C illuminates that the latter procedure is not completely transformed into La_2O_3 (see Fig. 7).

For **6**, the formula of weight loss begins at the start of the experiment, and the removal of lattice water molecules is accomplished at 115 °C. The calculated value for nine lattice–water molecules (14.58%) is in excellent agreement with the experimental result (14.65%). The dehydrated compound is then stable up to the abstraction of the coordinated water molecules which begins at 130 °C and accomplishes at 180 °C. The experimental value (8.93%) is lower than the calculated value for the loss of eight coordinated water molecules (12.96%) suggesting that two water molecules are still coordinated to the Y^{3+} center. Similar to **1**, the residue is a not pure Y_2O_3.

In addition, the analyses of thermal stability of the two samples are also investigated by DSC-measurement with a heating rate of 10 °C min^{-1} from 30 to 500 °C (see Fig. 6). Figure 7 shows the effects of calcination temperatures on their structures. From Fig. 6, the endothermic peak at 93 °C for **1** is due to loss of lattice and coordinated water molecules. The second peak is exothermic, which is corresponding to the decomposition process. The process still lasts until 500 °C. With increasing calcination temperature (from 50 to 140 °C), peak intensities and widths do not change obviously. The phenomenon reveals that the dehydrated process has little influence on structure until 200 °C, at the moment the partially dehydrated **1** begins to collapse.

For **6**, the first and second peaks are endothermic at 83, 151 °C which are corresponding to loss of lattice and coordinated water molecules. The third peak is exothermic, which is corresponding to the decomposition process. The process still continues until 500 °C. The phenomenon is consistent with slight changes including peak intensities decrease and widths become broad from 50 to 140 °C in PXRD graph. The flat curve implies that the partially dehydrated **6** begins to collapse above 200 °C.

For **1** and **6**, owing to the strong π–π stacking and hydrogen bonds interactions, the removal of coordinated water molecules takes place above 100 °C. Moreover, the slightly different thermal behavior can be attributed to the different numbers of coordinated water molecules in La^{3+}/Y^{3+}, which further confirm that their structures are different.

Conclusions

In summary, we synthesized six new compounds of $[La(H_2O)_9](m\text{-BDTH})_3{\cdot}9(H_2O)$ (**1**), $[Lu(H_2O)_8](m\text{-BDTH})_3{\cdot}9(H_2O)$ (**2**), $[Yb(H_2O)_8](m\text{-BDTH})_3{\cdot}9(H_2O)$ (**3**), $[Er(H_2O)_8](m\text{-BDTH})_3{\cdot}9(H_2O)$ (**4**), $[Ho(H_2O)_8](m\text{-BDTH})_3{\cdot}9(H_2O)$ (**5**), and $[Y(H_2O)_8](m\text{-BDTH})_3{\cdot}9(H_2O)$ (**6**) under hydrothermal conditions. Powder X-ray diffraction indicates that compounds **2**–**6** are isomorphous. We have presented a detailed examination of the structures and properties of a new family of 2-D hydrophobic organic layers of π-stacked and hydrogen-bonded $(m\text{-BDTH})^-$ which are separated by hydrophilic $[Ln(H_2O)_n]^{3+}$ cationic pillars. TG in conjunction with DSC and PXRD graphs reveal effects of water molecules on thermal stability. In addition, for **1** and **6**, the powders are amorphous above 200 °C, the partially dehydrated compounds begin to collapse.

Caution

$m\text{-BDTH}_2$ in its dehydrated form is insensitive to shock and friction, the lanthanide compounds with $m\text{-BDTH}_2$ are energetic. Appropriate safety precautions should be taken.

Supplementary material

Crystallographic data for the structural analyses have been deposited with the Cambridge Crystallographic Data Centre, CCDC no. 803363 and 803364 for **1** and **6**. Copies of this information may be obtained free of charge on application to CCDC (fax: 0044-1223-336-033; e-mail: deposit@ccdc.cam.ac.uk or http://www.ccdc.cam.ac.uk).

Acknowledgements We gratefully acknowledge the financial support from the National Natural Science Foundation of China (grant no. 20873100), and the Nature Science Foundation of Shaanxi Province (grant nos. FF10091 and SJ08B09).

References

1. Lehn JM. Perspectives in supramolecular chemistry-from molecular recognition towards molecular information processing and self-organization. Angew Chem Int Ed. 1990;29:1304–19.
2. Batten SR. Topology of interpenetration. CrystEngComm. 2001;3:67–72.
3. Braga D, Grepioni F. Intermolecular interactions in nonorganic crystal engineering. Acc Chem Res. 2000;33:601–8.
4. Mooibroek TJ, Gamez P, Reedijk J. Lone pair–π interactions: a new supramolecular bond? CrystEngComm. 2008;10:1501–15.
5. Chen SP, Li N, Wei Q, Gao SL. Synthesis, structure analysis and thermodynamics of $[Ni(H_2O)_4(TO)_2](NO_3)_2{\cdot}2H_2O$ (TO = 1,2,4-triazole-5-one). J Therm Anal Calorim. 2010;100:1115–20.
6. Hosseini MW. Molecular tectonics: from molecular recognition of anions to molecular networks. Coord Chem Rev. 2003;240:157–66.
7. Ballbh A, Trivedi DR, Dastidar P, Suresh E. Hydrogen bonded supramolecular network in organic salts: crystal structures of acid–base salts of dicarboxylic acids and amines. CrystEngComm. 2002;4:135–42.
8. Burrows AD, Chan CW, Chowdhry MM, McGrady JE, Mingos DMP. Multidimensional crystal engineering of bifunctional metal complexes containing complementary triple hydrogen bonds. Chem Soc Rev. 1995;24:329–39.
9. Logvinenko V. Stability of supramolecular compounds under heating. J Therm Anal Calorim. 2010;101:577–83.
10. Kawata S, Kumagai H, Adachi K, Kitagawa S. Novel layered structures constructed from metal(II)–chloranilate monomer compounds. J Chem Soc Dalton Trans. 2000;14:2409–17.
11. Liu K, Brown MG, Carter C, Saykally RJ, Gregory JK, Clary DC. Characterization of a cage form of the water hexamer. Nature. 1996;381:501–3.
12. Nauta K, Miller RE. Formation of cyclic water hexamer in liquid helium: the smallest piece of ice. Science. 2000;287:293–5.
13. Butler RN. In: Katritzky AR, Rees CW, Scriven EFV, editors. Comprehensive heterocyclic chemistry II. Oxford: Pergamon Press; 1996. pp. 621–2.
14. Herr RJ. 5-Substituted-1*H*-tetrazoles as carboxylic acid isosteres: medicinal chemistry and synthetic methods. Bioorg Med Chem. 2002;10:3379–93.
15. Eddaoudi M, Moler DB, Li HL, Chen BL, Reineke TM, O'Keeffe M, Yaghi OM. Modular chemistry: secondary building units as a basis for the design of highly porous and robust metal–organic carboxylate frameworks. Acc Chem Res. 2001;34:319–30.
16. Moulton B, Zaworotko MJ. From molecules to crystal engineering: supramolecular isomerism and polymorphism in network solids. Chem Rev. 2001;101:1629–58.
17. Kitagawa S, Kitaura R, Noro S. Functional porous coordination polymers. Angew Chem Int Ed. 2004;43:2334–75.
18. Zhang JP, Lin YY, Huang XC, Chen XM. Molecular chairs, zippers, zigzag and helical chains: chemical enumeration of supramolecular isomerism based on a predesigned metal–organic building-block. Chem Commun. 2005;40:1258–60.
19. Kostakis GE, Abbas G, Anson CE, Powell AK. A new class of 3-D porous framework: $[Ln(H_2O)_n]^{3+}$ ions act as pillars between π-stacked and H-bonded sheets of $(m\text{-BDTH})^-$ organic anions in $[Ln(H_2O)_n](m\text{-BDTH})_3{\cdot}9(H_2O)$(Ln = Pr, $n = 9$; Ln = Gd, $n = 8$). CrystEngComm. 2008;10:1117–9.
20. Sheldrick GM. SHELXS-97, program for X-ray crystal structure determination. Göttingen: Göttingen University; 1997.
21. Sheldrick GM. SHELXL-97, program for X-ray crystal structure refinement. Göttingen: Göttingen University; 1997.
22. Fleming A, Kelleher F, Mahon MF, McGinley J, Prajapati V. Reactions of bis(tetrazole)phenylenes. Surprising formation of vinyl compounds from alkyl halides. Tetrahedron. 2005;61:7002–11.
23. Zhang JP, Chen XM. Crystal engineering of binary metal imidazolate and triazolate frameworks. Chem Commun. 2006;41:1689–99.
24. Ouellette W, Hudson BS, Zubieta J. Hydrothermal and structural chemistry of the zinc(II)- and cadmium(II)-1,2,4-triazolate systems. Inorg Chem. 2007;46:4887–904.